Journal of The Electrochemical Society, **151** (3) B179-B187 (2004)
0013-4651/2004/151(3)/B179/9/$7.00 © The Electrochemical Society, Inc.

Electrochemical Studies of AC/DC Anodized Mg Alloy in NaCl Solution

S. J. Xia,[a,*] R. Yue,[a] R. G. Rateick, Jr.,[b] and V. I. Birss[a,*,z]

[a]*Department of Chemistry, The University of Calgary, Calgary, Alberta T2N 1N4, Canada*
[b]*Honeywell Engineering, Systems and Services, South Bend, Indiana 46620, USA*

The corrosion behavior of a Mg-based alloy, WE43, ac/dc anodized using a waveform involving a final period of current decay in an alkaline silicate solution, has been investigated using electrochemical impedance spectroscopy during exposure to a 0.86 M NaCl solution. The change of the oxide film morphology with immersion time was also examined using scanning electron microscopy. Anodization of the WE43 alloy significantly improves its corrosion resistance and greatly increases the time to pitting in the NaCl solution, which for air-formed films is in the range 2-3 h. By fitting the impedance data to a two-time-constant equivalent circuit and by tracking the open-circuit potential, it is demonstrated that film hydration initially decreases the corrosion resistance, followed by an increase in the resistance due to the gradual conversion of MgO to $Mg(OH)_2$, which leads to partial blocking of the film pores. During this time period, the underlying barrier film is slowly thinned and/or penetrated by chloride ions, consistent with its increasing capacitance and decreasing resistance, ultimately leading to a loss in corrosion resistance. Overall, both the porous and barrier oxide layers contribute to the corrosion protection of WE43, and the higher the voltage and the longer the time of current decay in the latter stages of anodization, the lower the alloy corrosion susceptibility.
 [DOI: 10.1149/1.1646139]

Manuscript submitted June 19, 2003; revised manuscript received October 1, 2003. Available electronically February 5, 2004.

The attractive future of Mg and Mg alloys arises from their light density, high strength-to-weight ratio, good mechanical properties, and excellent castability.[1,2] There are two major classes of Mg alloys, the first containing 2-10% Al also containing minor additions of Zn and Mn, and the second involving Mg alloyed with various elements other than Al. All alloys in the second group contain Zr, which imparts a fine grain structure, thus improving the mechanical properties. The WE43 alloy belongs to this second group and has many unique features that include high corrosion resistance, long-term stability at temperatures up to 250°C, and very good yield and tensile strength.[3-5] While the corrosion resistance of WE43 can be as good as that of some cast Al alloys, it still needs significant improvement for application in aerospace and other areas.

The general corrosion of Mg occurs due to the lack of a protective passive oxide film. In addition, the presence of other elements having a low hydrogen overpotential, such as Fe, Cu, or Ni, further enhances Mg corrosion via galvanic coupling.[6] It should be noted that WE43 is superior to other Mg alloys in its corrosion resistance.[7] Normally, Mg and its alloys form a mixed surface film of $Mg(OH)_2$ and MgO when exposed to humid air.[7] This film has excellent stability and provides reasonable corrosion resistance in air at room temperature, although it is porous and permeable to water in aqueous environments.[8] In most cases, hydrogen evolution is the main cathodic reaction associated with Mg corrosion. The film formation mechanism for Mg and its alloys is complex and the role of its alloying elements is still not clearly understood.[9] For example, the addition of Al stabilizes Mg oxide, even though the oxide layer is thinned as the amount of Al present is increased.[10] Also, the beneficial effect on the corrosion resistance of Mg-Al alloys of adding Mn is achieved by decreasing the galvanic potential difference between the intermetallic particles and the surrounding matrix.[11]

Improvements in the corrosion resistance of Mg and its alloys can be achieved by the application of a chemical conversion coating, by its anodization,[12-19] by anodization followed by sealing with an organic resin,[20] and by Parylene coating.[21] Various chemical conversion processes, such as the Cr-Mn or the chromate (Dow 7[13]) approach, in particular, are currently in use. Due to the porosity of these chemical conversion coatings, their corrosion resistance is not sufficiently high in aggressive media. Post-treatments, such as surface sealing and painting, are necessary when more protective coatings are required. Excellent corrosion resistance has been achieved in 0.5 M NaCl by the application of one to three layers of epoxy resin on Cr-Mn conversion-coated Mg AZ31 alloy.[20]

Anodic oxidation can also produce an oxide film that has a reasonable corrosion resistance and also provides an excellent paint or polymer coating base. These anodic oxide films usually have good hardness and abrasion resistance. Two common anodization approaches employed in the past 30 years are the Dow 17[13] and HAE[12] processes, which rely on spark formation on the anode to develop ceramic-like films. The Dow 17 method is carried out in an aqueous acidic solution containing phosphate, fluoride, and chromate, whereas the HAE process involves the use of an aqueous alkaline electrolyte containing phosphate, fluoride, manganate, and Al ions.[12] The Dow 17 method produces an excellent anodic oxide film with a high corrosion resistance, but it involves the use of chromate, which is environmentally harmful and is being gradually restricted. The HAE anodized oxide film without any sealing does not survive exposure to 0.5 M NaCl for even 1 day.

Recently, several other proprietary processes for the spark-anodization of Mg alloys have been developed.[14-19] Hawkins[22] examined several of these protection approaches and found that a coating, anodized in an alkaline silicate solution,[16] exhibited superior corrosion resistance as compared to that of Dow 17. The corrosion resistance of these anodized Mg alloys was evaluated by salt-fog testing, and an analysis of the corrosion mechanism was not provided.

In our previous paper,[23] an alkaline silicate electrolyte was employed to anodize the WE43 alloy. The oxide film, formed by using a novel waveform (an initially high-dc anodic voltage, followed by a nonlinear ramp, with a continuously superimposed ac voltage[23]) to generate sparks, resulted in the formation of a ceramic-like film on the alloy surface. This film was found to be composed of two layers, an outer porous and an inner barrier oxide film. The pores in the porous layer were seen to be somewhat interconnected, but did not traverse through to the barrier layer or to the WE43 substrate.[23] The total thickness of the anodic oxide film was found to be proportional to the final anodic voltage.[23] The coating thus formed in the silicate electrolyte containing fluoride ions was found to be composed of MgO, $Mg(OH)_2$, SiO_2, and MgF_2, with a molar ratio of 16:8:11:3.

The main objective of the present paper is to establish the corrosion resistance of anodized WE43 specimens in 0.86 M NaCl solution using the impedance technique as a function of the anodization parameters employed. Related to this, our goals were to determine the processes involved in oxide film breakdown and to correlate these with both the impedance data and with oxide film thickness and morphology, as determined from scanning electron microscopy (SEM) analyses.

* Electrochemical Society Active Member.
z E-mail: birss@ucalgary.ca

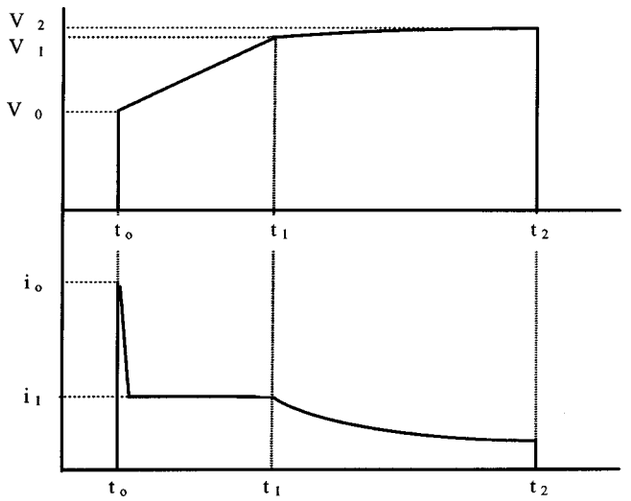

Figure 1. Waveform employed in WE43 anodization. Initial voltage (V_o) is 190 V.

Experimental

Materials and anodization procedure.—The Mg alloy, WE43, was supplied by Magnesium Elektron, Ltd., and cast by Chicago Magnesium. From the material certification, the composition (weight percentage) of the alloy was as follows: Mg (92), Y (3.73), Nd (2.41), Zr (0.53), Re (1.1), Zn (0.032), Li (0.125), Mn (0.018), and Cu (0.001).[23] Disk specimens, 10 mm diam and 5 mm thick, were cut from the cast WE43 alloy, and their surfaces were then single-point machined, followed by mechanical polishing using abrasive paper and coating with corrosion protection oil, purchased from LPS laboratories, Inc., to ensure corrosion protection during storage.

Prior to anodization, the WE43 disks were cleaned with ethanol to remove the oil and were then dried in air. The anodization of the WE43 disks, mounted vertically in the cell to allow easy gas evolution, was carried out in a bath containing sodium silicate, potassium fluoride, and potassium hydroxide.[16] The cathode (counter electrode, CE) was a 10 cm^2 316 stainless steel sheet and was located near the base of the cell. The bath temperature was kept between 10 and 20°C during the anodizing step. The anodization process was accomplished using a relatively high-voltage rectifier which supplied a combination of alternating (ac, 60 Hz sine wave) and dc power to the electrochemical cell. The anodization current densities and voltages, reported in the present paper, represent the sum of the dc and ac components.

In the present investigation, only waveform A[23] was employed in the anodization of WE43 specimens. In waveform A (Fig. 1), a minimum voltage of 190 V was initially applied to the disk specimens, causing the current density to spike to 50-60 mA/cm^2 (i_0), decaying over 10-30 s to the desired current (i_1). Then an ac voltage, maintained at *ca.* 20% of dc, was superimposed on the dc voltage and the dc/ac voltages were increased together with time to maintain a specific constant current density (i_1) for a period of time t_1. This was followed by a period (t_1-t_2) of decreasing current to produce an oxide film of a particular thickness. The anodization of the WE43 specimens using this approach is indicated as ''anodized at i_1 for t_1, Δt'' ($\Delta t = t_2$-t_1) in the text. The sides of the anodized disk and one of its faces were then wrapped with Teflon tape and then coated with epoxy resin, leaving only one face (0.78 cm^2) exposed to solution during corrosion testing in 0.86 M NaCl.

Electrochemical measurements and SEM analysis.—The impedance measurements were carried out using a Solartron 1255 frequency response analyzer connected to a Solartron 1286 electrochemical interface. In this work, the ac frequencies ranged from 100 kHz to 0.1 Hz, 12 points per decade, with a polarization amplitude of 10 mV (root mean square; rms) around the open-circuit potential (OCP). Impedance measurements and data acquisition were achieved using Zplot software.

A saturated calomel electrode (SCE) was used as the reference electrode (RE) in all of this work, and a large-area Pt gauze electrode was used as the CE for the ac impedance experiments. To minimize the phase shift at high frequencies, which is caused by the SCE, a pseudo-reference electrode (Pt wire) was also immersed in solution and was connected to the lead of the RE via a 6.8 μF capacitor.[20]

All solutions used in this work were prepared from analytical-grade reagents and triply distilled water (obtained using a Corning MP6A Mega-Pure distillation system). The solution used for the electrochemical evaluation of the coating was 0.86 M NaCl (*i.e.*, 5 wt % NaCl), consistent with the typical solution used in salt fog spray tests (as per ASTM B177). No attempt was made to deaerate any of the solutions. All experiments involving coating evaluation were performed at room temperature, *i.e.*, 20-22°C.

The surface of the anodized WE43 alloy specimens, both before and after corrosion testing, was examined by SEM using a JSM 6300 V (JEOL) instrument equipped with energy-dispersive X-ray (EDX) analysis facilities.

Results and Discussion

Behavior of bare (nonanodized) WE43 in NaCl solution.—When a bare WE43 specimen is initially immersed in 0.86 M NaCl, hydrogen evolution is seen to occur immediately and the surface becomes covered with bubbles, indicating that Mg is being oxidized, suggested to occur as follows[24]

$$Mg + 2H_2O = Mg(OH)_2 + H_2 \quad [1]$$

In neutral salt solutions, $Mg(OH)_2$ is predicted to be thermodynamically more stable than MgO.[24] The hydrogen bubbles nucleate and are periodically released from the surface, which becomes gray and rough in appearance with time.

In order to determine the corrosion resistance of the bare WE43 specimens, ac impedance data were collected at the OCP. A typical set of impedance data is shown in Fig. 2, in both the Nyquist and Bode representations, along with an overlay obtained by best-fitting to the equivalent circuit shown in the inset. The circuit consists of two time constants (two *R-CPE* units in series), *i.e.*, $R_s(R_1CPE_1) \times (R_2CPE_2)$, where R_S is the solution resistance between the WE43 specimen and the RE. In these experiments, R_s is in the range 5-10 Ω, while R_1 and R_2, related to the oxide film/charge-transfer resistance, were found to vary from 100 to 1000 Ω. The CPEs in Fig. 2 represent constant phase elements (a CPE reflects the dispersion of a capacitive element around a central value[25]), with the relationship between a capacitor (C) and a CPE[25] being as follows

$$j\omega C = (j\omega)^n CPE \quad [2]$$

For $n = 0$, a CPE is a resistor, while for $n = 1$, a CPE represents a perfect capacitor. When n is between 0 and 1, its value can provide information about diffusion phenomena, surface morphology, and other dissipative processes.[26,27] When $n = 0.5$, for example, a CPE represents a Warburg diffusion element.

The resistance at low frequencies, R_{1f}, which can be obtained directly from the raw data, is very similar to the sum of R_1 and R_2, obtained by equivalent circuit fitting, and can be considered as an indication of the corrosion resistance of the sample. Figure 3 shows the OCP and the low-frequency resistance (R_{1f}), equal to the sum of R_1 and R_2, as a function of immersion time of the bare WE43 specimen in 0.86 M NaCl. It can be seen that the OCP increases from −2.0 V at 5 s to −1.75 V after 1 h, and then increases more slowly until pitting occurs after 2 h. Over this same time period, the corrosion resistance of the WE43 electrode increases with immersion time, from 750 Ω at 5 s to 2000 Ω after 1.5 h, after which it

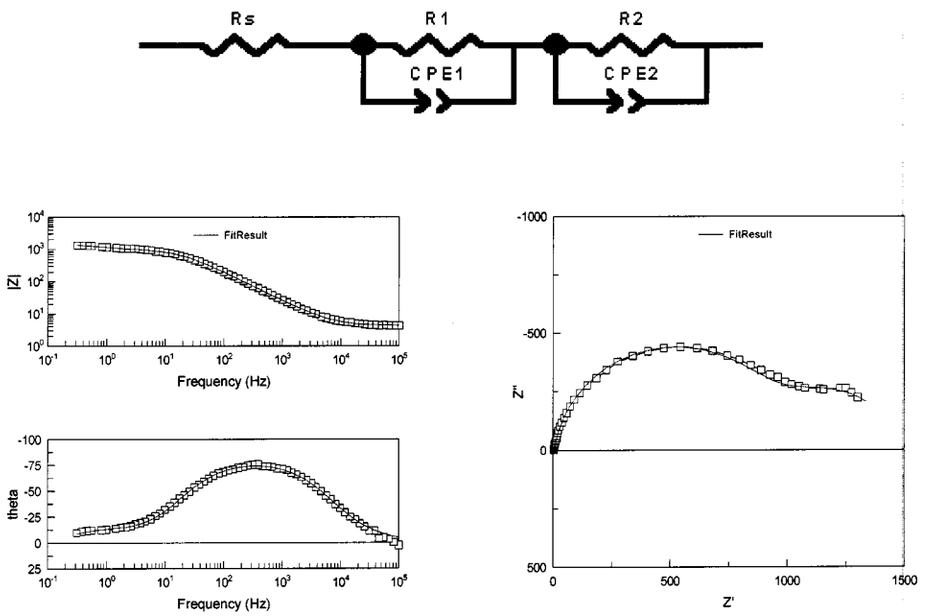

Figure 2. Experimental and simulated Bode and Nyquist plots of bare WE43 specimen after 20 min of immersion in 0.86 M NaCl solution. Insert: equivalent circuit used for impedance data fitting.

drops slowly. However, when pitting commences, the OCP shifts positively from −1.75 to −1.65 V, and the resistance decreased rapidly to 200 Ω in 20 min. Once pitting initiated, a white precipitate, likely $Mg(OH)_2$, was seen to form at the pits and to fall into solution, depositing on the base of the cell, and the alloy surface became porous and gray in color.

A positive shift of the OCP with exposure time in NaCl solution can be interpreted as reflecting surface passivation, *e.g.*, due to the formation of a Mg oxide film on the WE43 sample. However, the OCP shifted negatively from −1.80 to −1.86 V once some of the H_2 bubbles deposited on the surface were dislodged, and then shifted positively again as more H_2 bubbles formed. When the H_2 bubbles were removed, the corrosion resistance also changed, decreasing from 1500 to 780 Ω. These results indicate that the increase of the corrosion resistance and the positive shift of the OCP may at least in part be related to the blocking of the surface by hydrogen, and not due only to passivation by an oxide film.

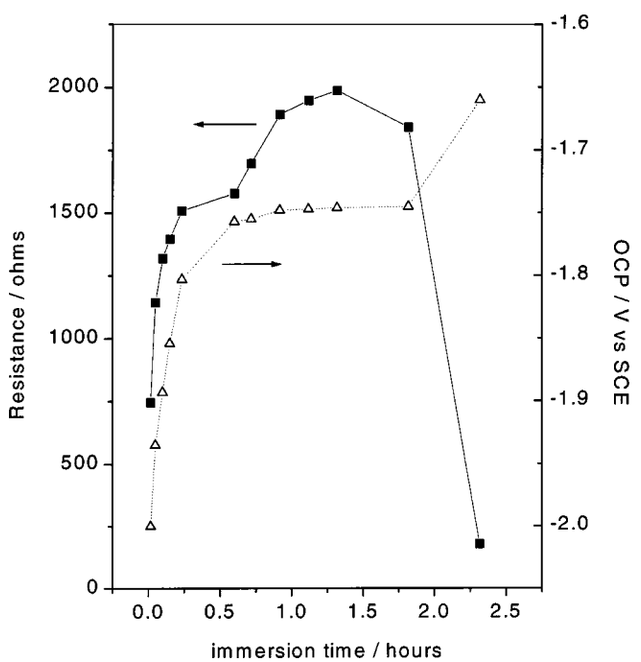

Figure 3. Development of (· · · ·) OCP and (——) corrosion resistance with immersion time in 0.86 M NaCl solution for bare WE43 specimen.

After *ca.* 1.5 h in the NaCl solution, the corrosion resistance decreased rapidly, while the OCP shifted positively with exposure time (Fig. 3). However, a low-frequency inductive loop, indicative of pitting corrosion,[28] was not seen in the impedance data until the pits could be seen visually on the surface. Once pitting had initiated, the OCP tended to stabilize at −1.60 V and the corrosion resistance decreased to *ca.* 20 Ω. In addition, white precipitate was seen building up in the solution with immersion time, likely indicating the formation of Mg oxide/hydroxide. Afterward, the WE43 surface was seen to be porous and deep pits, which were difficult to remove by subsequent polishing, were present.

Corrosion behavior of anodized WE43 alloy.—As discussed in our previous paper,[23] the Mg oxide film thickness can be increased in the alkaline silicate solution by applying higher anodization voltages. Figure 4 shows the change in the electrode impedance (Bode plot) as a function of immersion time in the first 120 min in 0.86 M NaCl for the WE43 alloy, anodized at 30 mA/cm^2 using waveform A for 5,25 min. This code means that in the first 5 min a constant current of 30 mA/cm^2 was applied. After that the current was allowed to decay slowly with time until anodization was complete after 30 min. The final voltage and current were 408 V and 5 mA/cm^2, respectively, for this particular sample.

The impedance data obtained at short times (*e.g.*, 5 min) of immersion show that at frequencies above ~10 Hz, the phase angle remains almost constant at −87° and the magnitude of the impedance $|Z|$ increases linearly with $\log f$, typical of a capacitive response.[20] From 2 to 30 min, the phase angle at high frequencies decreases from −87 to −80° but still remains fairly capacitive in nature. Due to the difficulty of fitting this early time impedance data, which changed rapidly with time, a reliable equivalent circuit which could be fitted well to the data at all frequencies could not be identified. Therefore, the capacitance for these short times of immersion was determined only from the high-frequency data, using an equivalent circuit composed of the solution resistance and a film capacitance in series, and was found to be 10 nF.

The oxide film formed in the alkaline silicate solution is composed of an intact, inner barrier layer and an outer, porous film.[23] Assuming the film dielectric constant to be 9.6 for MgO,[29] the thick-

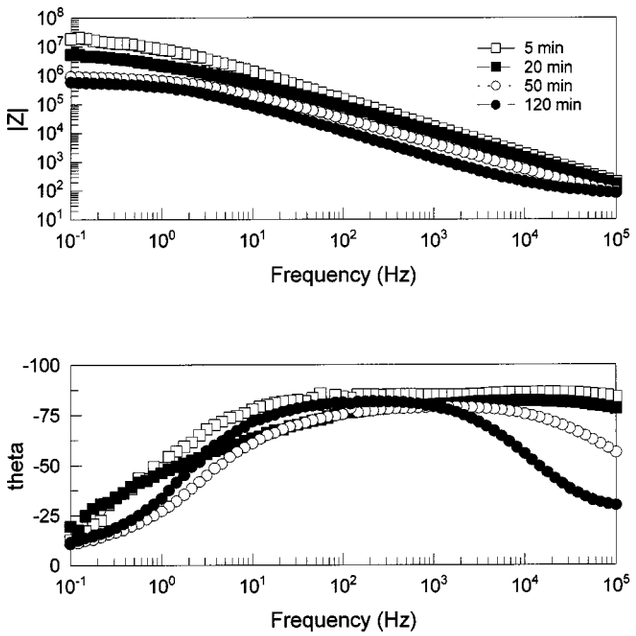

Figure 4. Change of Bode plots of WE43 specimen, anodized in alkaline silicate solution at 30 mA/cm^2 for 5,25 min, with immersion time in 0.86 M NaCl.

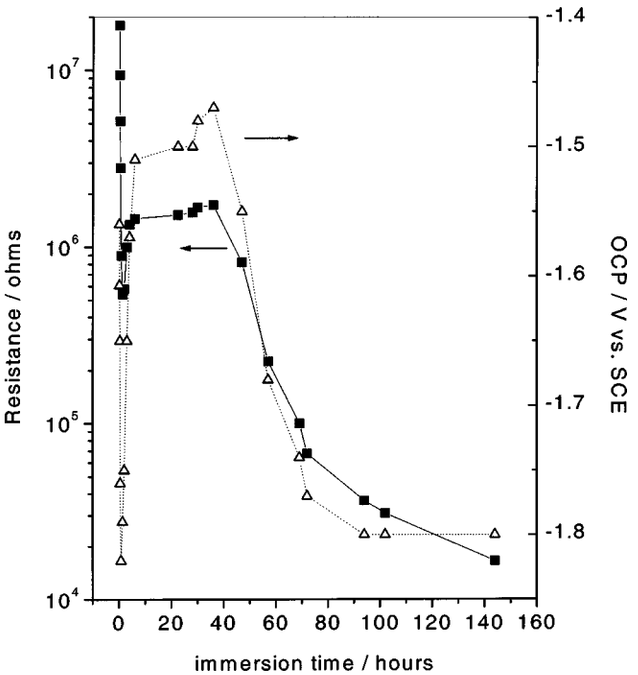

Figure 5. (——) Corrosion resistance and (· · · ·) OCP as a function of immersion time in 0.86 M NaCl for WE43 alloy, anodized in alkaline silicate solution at 30 mA/cm^2 for 5,25 min.

ness of the intact oxide film at these early stages of immersion in the NaCl solution is then predicted from the measured capacitance to be 0.90 μm. This is very close to the barrier oxide thickness, *ca.* 0.95 μm, seen from SEM analysis.[23] This shows clearly that the inner barrier film thickness can be determined just from the capacitance obtained from the impedance data at these early times of immersion in the NaCl solution.

The corrosion resistance of the anodized WE43 sample, determined from the magnitude of the impedance data (Fig. 4) at 0.1 Hz,[30] is shown in Fig. 5, along with the OCP, as a function of immersion time. It can be seen that the resistance is very much higher than for the bare sample (Fig. 3), as expected, *i.e.*, $>10^6$ Ω at short times (to more than 40 h) to $>10^4$ Ω at very long times. The corrosion resistance decreases rapidly from *ca.* 1.8×10^7 at 2 min to *ca.* 5.4×10^5 Ω after 1.5 h, while the OCP shifts negatively from −1.52 to −1.82 V. Figure 5 also shows that the trends of the corrosion resistance are mirrored completely by those of the OCP. After 1.5 h in the NaCl solution, the OCP shifts positively and the resistance increases with time until the highest OCP is reached at 30 h. After this, the OCP shifts negatively and the resistance decreases with immersion time, while after *ca.* 100 h the OCP stabilized at *ca.* −1.80 V while the resistance continues to decrease with time, reflective of further film breakdown.

It can be seen from Fig. 5 that the change in the OCP and corrosion resistance with immersion time can be separated into three different stages, these being in the 0-1.5, 1.5-30, and 30-150 h time periods. In the first stage, it is suggested that water and electrolyte penetrates the oxide film through the pores in the outer porous layer, reaching the interface between the inner barrier and the outer porous layer.[23] With the penetration of solution into the porous layer, the OCP shifts negatively from −1.52 V at 2 min to −1.82 V at 1.5 h, close to that of bare WE43 in NaCl solution, and the corrosion resistance decreases from 1.8×10^7 to 5.4×10^5 Ω. At this point, the NaCl solution is suggested to have reached the surface of the barrier layer, although some penetration to the underlying metal may also have occurred. Figure 6 shows the SEM image of the oxide surface, formed at 30 mA/cm^2 for 5,30 min, both prior to and after 1 h of immersion in NaCl. It can be seen that contact with the NaCl solution for this short period of time does not affect the morphology of the oxide surface, consistent with this explanation.

The anodic oxide film formed in alkaline silicate is composed of MgO, $Mg(OH)_2$, SiO_2, and MgF_2, with the molar ratio of MgO to $Mg(OH)_2$ being close to 2:1.[23] Thermodynamically, $Mg(OH)_2$ is more stable than MgO in aqueous solutions,[24] and MgO readily reacts with water to form $Mg(OH)_2$. However, the denser the MgO, the slower this conversion reaction has been reported to be.[24] Therefore, in the second stage in Fig. 5 it is suggested that MgO is being converted to the lower density $Mg(OH)_2$ film at the surface inside the pores of the oxide film. This could result in a partial blocking of the pores, because the molar volume of $Mg(OH)_2$ is larger than that of MgO, hence increasing the film resistance. In this time period, no H_2 evolution was seen and the color of the oxide film remained unchanged visually, indicating that the oxide morphology is not greatly altered during this time period and that little corrosive attack of the underlying Mg is occurring.

Figure 7 shows the SEM image of the anodized WE43 surface during this phase of exposure (after 5 h of immersion in NaCl), revealing no major changes in the film morphology other than the development of some cracks in the oxide in some areas, especially around the larger pores. The formation of $Mg(OH)_2$ inside the pores could change the mechanical stresses within the oxide film, causing some cracks to develop. The pore sizes appear to be the same as before corrosion testing (cf. with Fig. 6), indicating that the bulk of the film is very stable and that the reaction between MgO and water is slow.

After 30 h (third time period) of immersion in the NaCl solution, the color of the oxide film is seen visually to gradually change from white to gray, especially at the disk edge of the exposed area. It is not clear why the oxide film becomes darker with immersion time. This was also observed in salt fog testing. As in the second corrosion period, no H_2 evolution is observed and therefore, any newly formed $Mg(OH)_2$ was likely generated from the chemical reaction between MgO in the porous layer and water, and not from a corrosion reaction between Mg in the substrate and water or even oxygen. The barrier layer between the substrate and the porous layer still appears dense enough to block the penetration of water and NaCl to

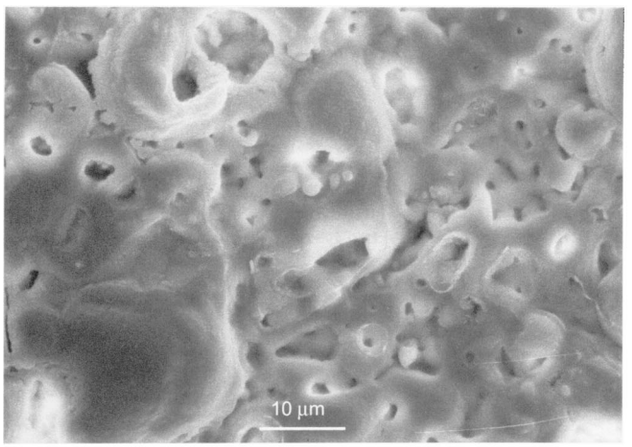

Figure 6. SEM images of anodized WE43 alloy: (a) before corrosion testing and (b) after 1 h of immersion in 0.86 M NaCl solution. The WE43 alloy was anodized in alkaline silicate solution at 30 mA/cm^2 for 5,25 min.

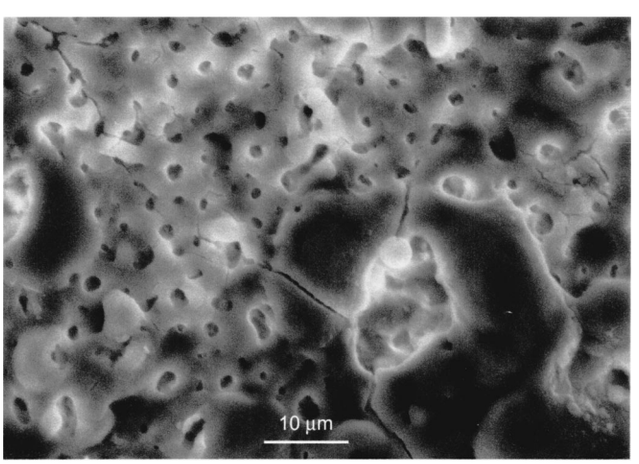

Figure 7. SEM image of anodized WE43 alloy after 5 h of immersion in 0.86 M NaCl solution. The WE43 alloy was anodized in alkaline silicate solution at 30 mA/cm^2 for 5,25 min.

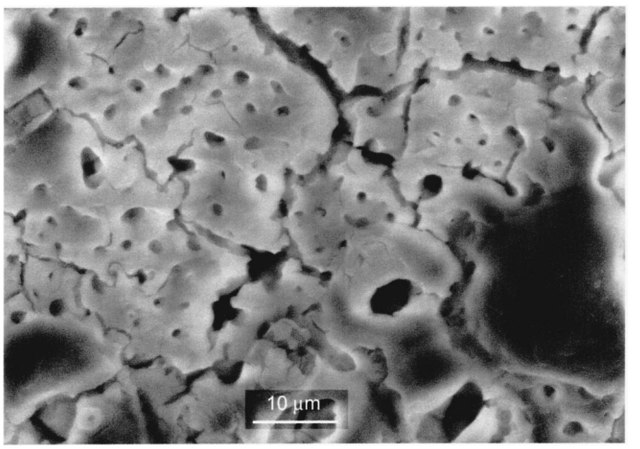

Figure 8. SEM image of anodized WE43 alloy after 55 h of immersion in 0.86 M NaCl solution. The WE43 alloy was anodized in alkaline silicate solution at 30 mA/cm^2 for 5,25 min.

the WE43 substrate. However, the corrosion resistance decreases with immersion time, and the OCP shifts negatively until a constant OCP is reached after 100 h (Fig. 5). The decrease of the corrosion resistance of the oxide film with immersion time may be the result of the formation of small pores or microcracks in the barrier layer. Alternatively, this may result from the slow thinning of the MgO barrier layer due to the reaction between the MgO at the barrier film surface and water at the base of the pores of the outer layer.

Figure 8 shows the SEM image of the oxide film after 55 h of immersion in NaCl. Two distinct characteristics, different from the morphologies discussed previously for shorter immersion times or before corrosion testing (Fig. 6a), are seen in Fig. 8. One is that the pores in the film seem to be filled with material, suggested to be newly formed $Mg(OH)_2$ from MgO. However, this material is likely quite porous and therefore would not be expected to serve as a protective barrier to chloride. The second change is the extended cracking of the oxide film. The width of the cracks is as large as 2 μm in some areas. No precipitate can be seen in the cracks from the SEM image. Therefore, the cracks in the film can provide another pathway for the penetration of NaCl solution to the barrier layer surface. The increasing exposure of barrier layer to solution could speed up the transformation of MgO to $Mg(OH)_2$, and the resulting volume expansion at the base of the porous layer could, in turn, cause further cracking of the porous layer.

Impedance data analysis.—The anodic oxide film, formed on the WE43 alloy by ac/dc anodization, has been shown to be composed of a thick, porous oxide [a mixture of MgO and $Mg(OH)_2$] and an underlying barrier layer, likely MgO.[23] During corrosion testing in NaCl solution, water can penetrate into the film pores and hydrate MgO, forming $Mg(OH)_2$,[24] which has a higher molar volume than MgO. It is very likely that the porous and barrier layers play a different role in the corrosion protection of the substrate. Electrochemical impedance spectroscopy (EIS) provides a powerful approach for the analysis of the change of the properties of each layer with immersion time through the fitting of experimental data to an equivalent circuit, such as shown in Fig. 2.

As a specific example, a detailed analysis of the impedance data, obtained for an oxide film formed at 30 mA/cm^2 for 5,25 min (final voltage $V_f = 408$ V; short time corrosion data is shown in Fig. 4), is carried out in the following section. As discussed previously, in the first 30 min of exposure to the NaCl solution, the data changed rapidly and a simple circuit involving only the solution resistance (R_s) and the film capacitance (CPE) in series was used to fit the high-frequency data. This led to a good estimate of the film capacitance, and hence its barrier thickness. The capacitance values thus

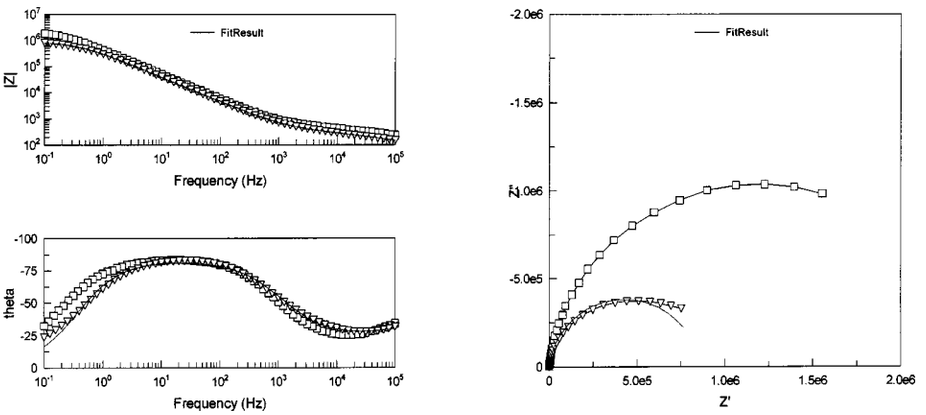

Figure 9. Experimental and simulated Bode and Nyquist plots of oxide film, formed at 30 mA/cm^2 for 5,25 min, after (□) 20 and (▽) 50 h of immersion in 0.86 M NaCl solution using an equivalent circuit shown in Fig. 2.

obtained were found to increase with immersion time, from 1.1 $\times$ 10^{-8} at 2 min to 2.8 $\times$ 10^{-8} F after 30 min, consistent with a decreasing film thickness, based on the equations for a parallel plate capacitor.[31] This is indicative of either dissolution of the layer or penetration of water and NaCl into defect sites within the barrier oxide film.

After 30 min in the NaCl solution, the impedance response stabilized greatly and the entire frequency range for this particular oxide film could be fitted to the equivalent circuit shown in Fig. 2, coded as $R_s(R_1CPE_1)(R_2CPE_2)$. Figure 9 shows the experimental and fitted data in both the Nyquist and Bode representations after 20 and 50 h of immersion in 0.86 M NaCl. R_s is found to remain close to constant, at *ca.* 15 Ω, with time in solution, as expected. The magnitude of each of the other elements in the equivalent circuit is shown in Fig. 10 as a function of immersion time in 0.86 M NaCl.

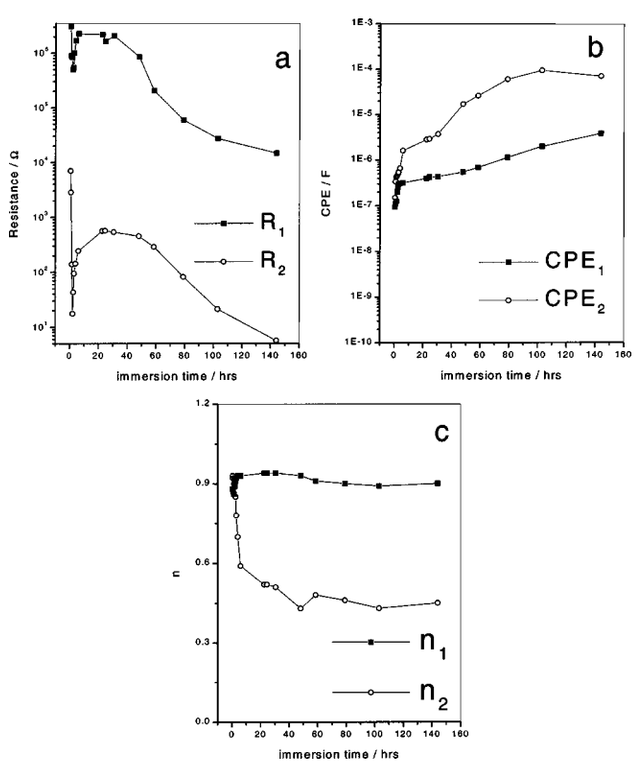

Figure 10. The change of each circuit element of a WE43 specimen, anodized in the alkaline silicate solution at 30 mA/cm^2 for 5,25 min, with immersion time in 0.86 M NaCl (see raw data in Fig. 9): (a) R_1, R_2 *vs.* time; (b) CPE_1, CPE_2 *vs.* time; and (c) n_1, n_2 *vs.* time.

Based partly on the values of the circuit elements (passivating oxide films typically have capacitances of 10^{-7} F or less and very high resistances, *e.g.*, 10^6 Ω or more[32]), and the fact that n_1 remains close to unity at all times, the R_1/CPE_1 pair is likely due to the barrier oxide film. Because its resistance is very high, the barrier oxide film controls the rate of the charge-transfer reaction during corrosion of the oxide-coated WE43 alloy and R_1 is very close in value to R_{1f} (also equivalent to the resistance obtained in linear polarization measurements, often used for corrosion rate measurements). The R_2/CPE_2 pair is suggested to represent the porous oxide layer, as discussed in more detail later.

It can be seen in Fig. 10a-c that the changes in the magnitude of the circuit elements with immersion time in 0.86 M NaCl can be divided into three periods. In the first period (0.5-2 h), R_1 and R_2 decrease rapidly with time, CPE_1 and CPE_2 increase, and n_1 and n_2 both remain constant and close to unity. From 2 to 30 h, R_1 and R_2 increase with time, CPE_1 and CPE_2 increase very slowly, and n_1 remains constant close to unity, but n_2 decreases. In the last period from 30 to 140 hours, R_1 and R_2 both decrease with time, CPE_1 and CPE_2 generally increase further, and n_1 remains constant and close to unity, but n_2 decreases slowly and reaches a steady-state value of ~0.45 after *ca.* 50 h.

In the first period, the decrease in R_1 and increase in CPE_1 could indicate that the barrier oxide film is becoming thinner. It is also likely that these changes in the properties of the oxide film are due to the formation of tiny pores and cracks in the barrier oxide film, with time of exposure to NaCl. The increase in CPE_1 and the decrease of R_1 could also be related to the gradual hydration of the surface of the MgO barrier layer with the penetration of water and NaCl into the pores of the overlying oxide film, forming a porous, poorly protecting $Mg(OH)_2$ surface layer on the barrier film.

In terms of R_2 and CPE_2 in this first period of time (Fig. 10), the decrease in R_2 is suggested to reflect an increase in the porous film conductivity, as the pores become saturated with the NaCl solution. The increase in CPE_2 may be caused by an increase in the interfacial area between the porous film and the solution, as its surface becomes hydrated and as the film cracks with time.[23]

From 2 to 30 hours, Fig. 10a shows that both R_1 and R_2 increase with immersion time, while CPE_1 and CPE_2 (Fig. 10b) increase and then stabilize. It is suggested that over this period of time, $Mg(OH)_2$ begins to form, due to the slow hydration of MgO, thus sealing or blocking some of the pores in the outer oxide film (and/or the barrier film), as its molar volume is higher than that of MgO. The resulting decrease in film porosity thus shifts the OCP positively (Fig. 5) and increases the overall film resistance. During this time period, the outer regions of the barrier film may be further hydrated or penetrated by chloride, although not significantly, explaining the almost unchanging trends in CPE_1. Indeed, n_1 remains close to unity, indicative of the retention of an intact layer of barrier

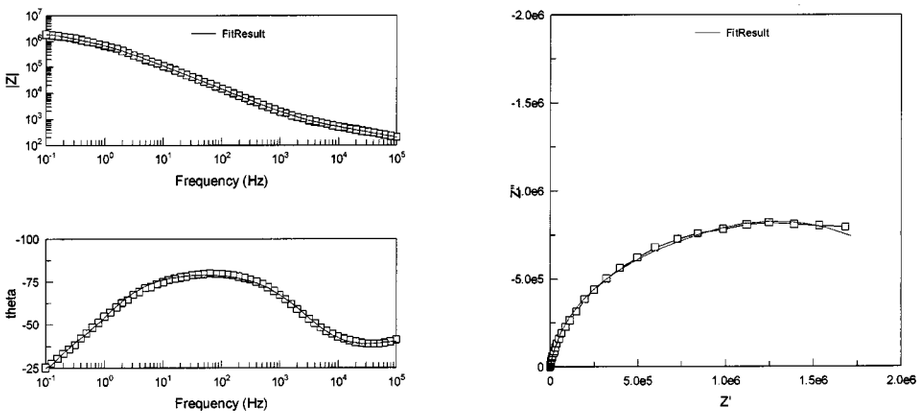

Figure 11. Experimental and simulated Bode and Nyquist plots of oxide film, formed at 30 mA/cm^2 for 5,15 min, after 20 h of immersion in 0.86 M NaCl solution using an equivalent circuit shown in Fig. 2.

film. The porous film likely is further altered during this time period, due to the formation of $Mg(OH)_2$ within its pores, thus leading to an increased interfacial area and CPE_2. Interestingly, n_2 decreases from 0.95 to *ca.* 0.50 after 30 h. This is consistent with the development of a very rough surface, or can indicate that the diffusion of reactants or products of the corrosion reaction within the pores of the outer oxide layer is rate controlling.

After about 30 h, R_1 and R_2 begin to decrease with immersion time, while CPE_1 and CPE_2 increase correspondingly. As shown in Fig. 6-8, with longer immersion times in 0.86 M NaCl, both the number and size of cracks in the film increase, likely due to the formation of the lower density $Mg(OH)_2$. With the formation of cracks, the effective surface area of the film increases, and the barrier layer becomes increasingly exposed to solution and hydrated. The fact that the n_1 value remains close to unity indicates that some intact barrier film is retained, even after 140 h in the salt solution.

Effect of final anodization voltage on corrosion behavior of ac/dc anodized WE43.—It has been found that the outer oxide pore size and distribution, as well as the barrier oxide film thickness, depend mainly on the final dc and ac voltages employed during ac/dc anodization.[23] At anodization voltages below *ca.* 390 V (sum of dc and ac), the film is not yet more than 10 μm thick and the pores are relatively uniform in size and do not exceed 4 μm diam. At higher voltages, thicker films are formed and the large and frequent sparks generated on the electrode surface can lead to high surface temperatures and partial sealing of the smaller (0.5-4 μm) pores. However, this type of sparking also leads to the formation of some very large pores, in the range of 6-15 μm diam,[23] which could potentially shorten the lifetime of these films in practice.

For an anodic oxide film formed at 30 mA/cm^2 for 5,15 min (V_f = 395 V), the experimental impedance data, measured in 5% NaCl after 20 h, are shown in Fig. 11. Similar to the impedance data in Fig. 9, the two-time-constant equivalent circuit, shown in Fig. 2, was found to fit the impedance data of Fig. 11 well. However, the data in the first 30 min were again relatively unstable, and therefore only the high-frequency data were fitted to a simple R_s-CPE equivalent circuit, yielding a capacitance which increased with immersion time, from 1.4×10^{-8} F at 2 min to 4.5×10^{-8} F at 30 min. This again indicates a decreasing barrier film thickness and/or penetration of NaCl solution into small pores/cracks in the film with time in the NaCl solution.

Figure 12 shows the change of each circuit element as a function of immersion time (>30 min) for the data set of Fig. 11. As was the case in Fig. 10, the data can be analyzed best in three time periods, 0.5-3, 3-15, and 15-120 h, and very similar trends are seen for both films. The differences include the fact that R_1 and R_2 reach their first minimum after 3 h for the 5,15 (V_f = 395 V) film, *vs.* 2 h (Fig. 10) for the 5,25 min (V_f = 408 V) film. Also, the time between the minimum and maximum R values for both R_1 and R_2 is shorter for the 395 V film (Fig. 12) than for the 408 V film (Fig. 10). This is probably because the 408 V oxide film (Fig. 10) was found to have a greater number of large pores[23] than the 395 V film in Fig. 12. As discussed previously, the film resistance reaches a maximum after all the pores are filled with $Mg(OH)_2$, formed by the hydration of MgO. Therefore, for the anodic film containing the larger pores, a longer time to block the pores would be expected.

For WE43 anodization to only a relatively low final voltage, such as 384 V (4,2 min film), large pores were not seen in the oxide film.[23] The impedance data obtained in 5% NaCl under these conditions were also fitted using the two-time-constant equivalent circuit, shown in Fig. 2. A set of typical experimental data is plotted in Fig. 13, which also includes the corresponding fitted data. The results shown in Fig. 13 indicate that the two-time-constant equivalent

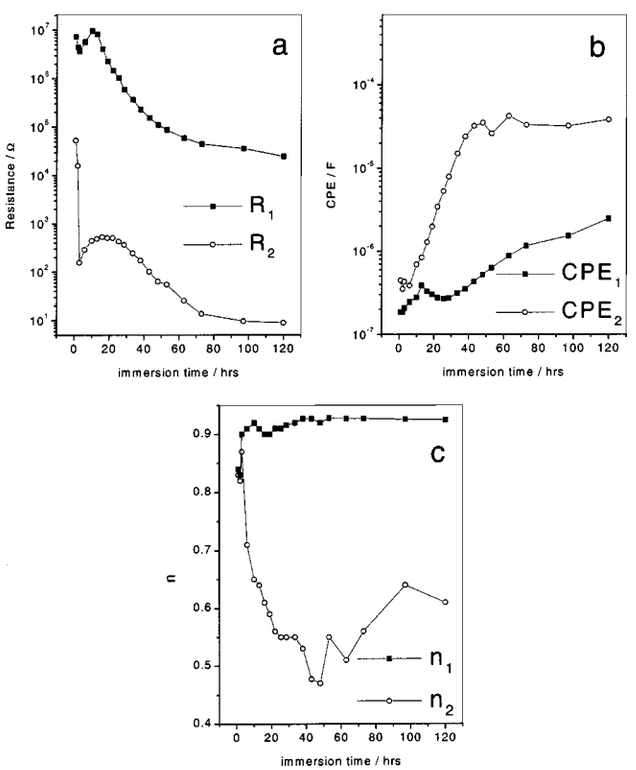

Figure 12. The change of each circuit element of a WE43 specimen, anodized in the alkaline silicate solution at 30 mA/cm^2 for 5,15 min, with immersion time in 0.86 M NaCl (see raw data of Fig. 11): (a) R_1, R_2 *vs.* time; (b) CPE_1, CPE_2 *vs.* time; and (c) n_1, n_2 *vs.* time.

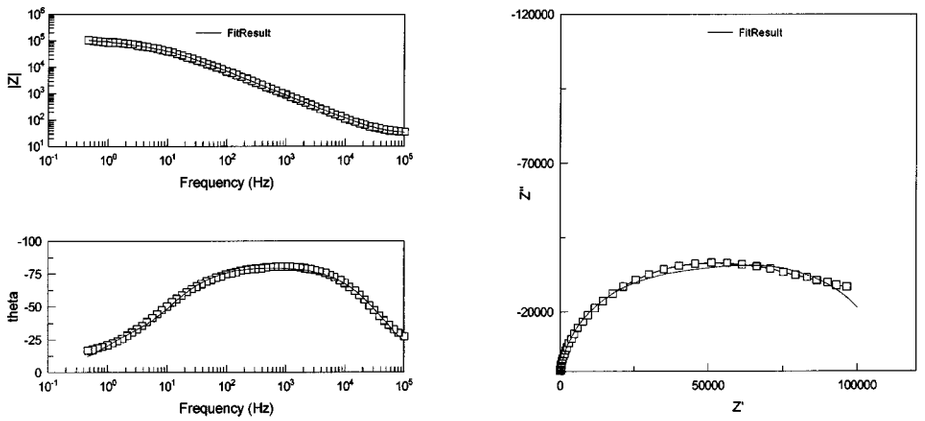

Figure 13. Experimental and simulated Bode and Nyquist plots of oxide film, formed at 30 mA/cm^2 for 4,2 min, after 20 h of immersion in 0.86 M NaCl solution using an equivalent circuit shown in Fig. 2.

circuit does fit the impedance data of the 384 V film very well. In this case, the barrier film capacitance in the first 30 min in 0.86 M NaCl, obtained by fitting the high-frequency data to the simple R_s-CPE equivalent circuit, was seen to increase from 1.8×10^{-8} F at 2 min to 8.0×10^{-8} F at 30 min. These values are higher than those obtained for the two oxides formed using longer anodization times and higher voltages (V_f = 395 and 408 V). This is consistent with a thinner barrier oxide film being formed at lower voltage, as seen from the cross-sectional SEM images.[23]

The change of each circuit element with immersion time for the 384 V film is shown in Fig. 14. Now R_1 and R_2 reach the first minimum after only 1.5 h and then go through a maximum after 5 h (Fig. 14), both much shorter times than for the films formed at higher final voltage (Fig. 10 and 12). Even though the pores of the 385 V film are smaller in diameter, the porous layer is thinner for the 384 V *vs.* 395 and 408 V films, so that the NaCl solution can penetrate it more rapidly. However, the rapid penetration of NaCl solution accelerates the hydration of MgO in the oxide film and the $Mg(OH)_2$ thus formed fills the small pores in shorter times. When the $Mg(OH)_2$ fills all the pores in the oxide film, the corrosion resistance reaches a maximum. One interesting difference for this film is that R_2, the resistance of the outer film, is *ca.* 100 times higher than for the films formed to higher anodizing voltages (Fig. 10 and 12). This would be consistent with the absence of large pores in the outer film in this case.[23] Notably, in the first 20 h of immersion in 0.86 M NaCl solution, R_1 is much higher than R_2 in Fig. 14, then becoming more similar in value. This could indicate that the porous film, represented by R_2, also provides corrosion protection when no large pores (above 6 μm diam) are present in the film.

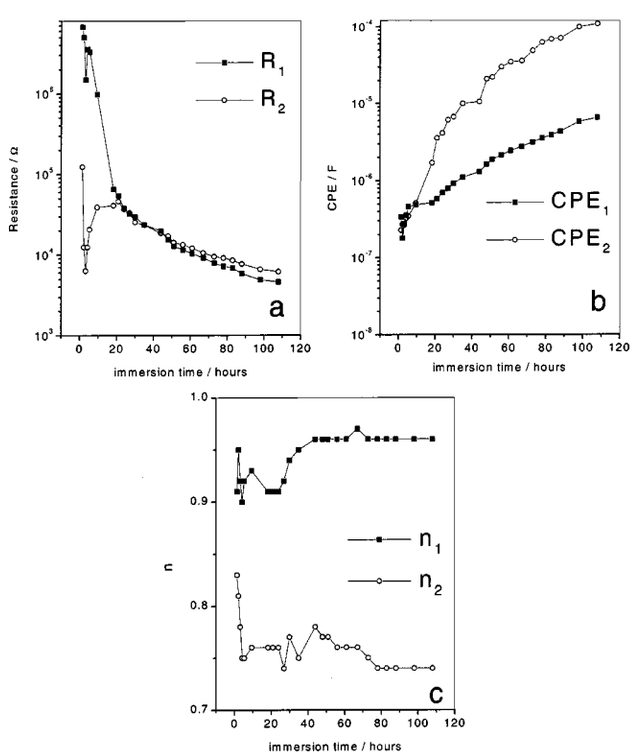

Figure 14. The change of each circuit element of a WE43 specimen, anodized in alkaline silicate solution at 30 mA/cm^2 for 4,2 min, with immersion time in 0.86 M NaCl (see raw data of Fig. 13): (a) R_1, R_2 *vs.* time; (b) CPE_1, CPE_2 *vs.* time; and (c) n_1, n_2 *vs.* time.

Unlike the behavior of CPE_2 in Fig. 10 and 12, CPE_2 in Fig. 14 continued to increase with immersion time until the experiment was terminated. Also, CPE_1 and CPE_2 are very similar in magnitude in the first 10 hours, after which CPE_1 becomes smaller than CPE_2. The more rapid increase of CPE_2 with immersion time could arise from the more rapid increase of the interfacial area between the porous film and the solution because of accelerated film wetting and cracking. These results indicate that the porous film plays an important role in corrosion protection when only small pores less than 6 μm diam are present in the oxide film.

Figure 15a shows a comparison of the corrosion resistance ($R = R_1 + R_2$) of three films, all formed at 30 mA/cm^2 and using waveform A, but varying in the time allowed for current decay and in the final voltage reached during anodization. It can clearly be seen that the corrosion resistance is notably higher the larger the final anodization voltage (the longer the period of current decay) during oxide growth. Furthermore, for the film formed at V_f = 384 V, a peak is not seen in the resistance/time plot, consistent with an altered breakdown mechanism. Figure 15b shows that the OCP values are more negative for these three films at any time the lower the V_f value is. Also, for the 384 V film, the OCP reaches a very low minimum near −1.95 V for a period of time, much more negative than for the other two oxide films. As a lower OCP value, together with a lower corrosion resistance, would be encountered only when the oxidation half-reaction is accelerated, based on corrosion theory, this indicates clearly that the oxide film formed at low V_f is less corrosion resistant.

Conclusions

Contrary to the case of bare WE43 specimens or of Mg samples oxidized only by exposure to water, excellent corrosion protection of the WE43 alloy can be achieved by ac/dc anodization in an alkaline silicate solution at high voltages (>350 V). No pitting of the anodized WE43 alloy surface in 0.86 M NaCl solution is then observed visually, even after more than 140 h of immersion.

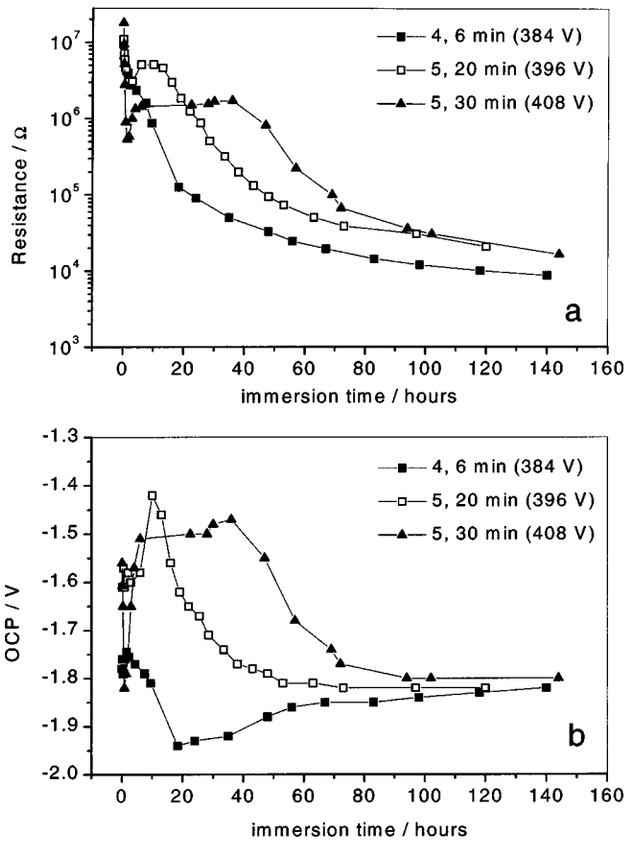

Figure 15. (a) Corrosion resistance and (b) OCP of three WE43 alloys, anodized at 30 mA/cm^2 for 4,2 min (V_f = 384 V, -■-), 5,15 min (V_f = 396 V, -□-), and 5,25 min (V_f = 408 V, -▲-) as a function of immersion time in 0.86 M NaCl.

The impedance technique was found to be an excellent approach for the corrosion testing of these anodized WE43 specimens. Indeed, an analysis of the impedance data collected in NaCl solutions showed that an equivalent circuit involving two time constants in series with the solution resistance, $R_s(R_1CPE_1)(R_2CPE_2)$, could be used to extract useful film characteristics from the raw impedance data. The resistance of the anodized WE43 specimens to corrosion could be evaluated from the sum of R_1 and R_2, or directly from the raw data from the low-frequency resistance. The oxide film formed on the ac/dc anodized WE43 alloy system was found to be composed of two layers, an outer porous oxide layer and an underlying thinner barrier oxide film using SEM. The R_1/CPE_1 pair was shown to depict the barrier oxide film, while R_2CPE_2 was argued to represent the porous oxide layer.

In the first approximately 30 min of immersion of the anodized WE43 specimens in 0.86 M NaCl, the thickness of the barrier layer, calculated from the capacitance at high frequencies, is in agreement with that obtained for a freshly formed oxide film from cross-sectional SEM images. After this, the changes in the corrosion resistance, the barrier film capacitance (CPE_1), and the OCP with immersion time can be separated into three periods. In the first period (typically $< ca.$ 2 h), the corrosion resistance and the OCP decreases, while CPE_1 increases. In the second phase (from 2 to about 30 h), the resistance and the OCP increases and CPE_1 increases, while in the third period (approximately $> ca.$ 30 h), the corrosion resistance and OCP decreases (and CPE_1 increases) with immersion time. These trends have been explained as reflecting the rapid initial penetration of solution through the porous outer film to the barrier layer in the first phase, followed by the hydration of MgO in the pores in the second. The resistance decrease at longer times (third stage) is likely due to the formation of cracks in the oxide film and the dissolution of $Mg(OH)_2$ in the pores and then into bulk solution.

Both the barrier and porous oxide film thickness increase with an increase in the period of time of current decay, during which the anodization voltage also increases further, resulting in an increase in the corrosion resistance of the WE43 alloy specimens. In general, the higher the final voltage, the higher the corrosion resistance of the oxide film. However, high voltages also lead to the formation of large pores, greater than 5 μm diam, in the outer film layer under these conditions. Allowing a long period of time of current decay also thickens the barrier film, enhancing the sample corrosion resistance which is dominated by the barrier film. For oxide films which do not contain large pores 5 μm diam or greater, *i.e.*, those formed at voltages less than *ca.* 385 V (short period of time of current decay, such as 5 min), the porous layer plays an important role in corrosion protection, similar to the barrier oxide film, after *ca.* 20 h in 0.86 M NaCl.

Acknowledgments

Financial support from Honeywell International is gratefully acknowledged. Special thanks are extended to the Honeywell Engineering, Systems & Services, South Bend Materials Technology Center, for the SEM analyses.

The University of Calgary assisted in meeting the publication costs of this article.

References

1. P. Greenfield, M&B Monograph ME/11, Mills & Boon, Ltd., London (1972).
2. I. J. Polmear, *Light Alloys: Metallurgy of the Light Metals*, Chap. 5, Edward Arnold, London (1981).
3. G. A. Fowler, J. F. King, and P. Lyon, *Corrosion Resistant Magnesium Alloys*, Magnesium Electron, Ltd., Swinton, Manchester, England (1990).
4. J. M. Arlhac and J. C. Chaize, Presented in *Aeromat '96 Conference*, American Society of Metals, Dayton, OH, June 1996.
5. MEL Data Sheet 467 A, "Elektron WE43," Aug 1987.
6. N. S. McIntyre and C. Chen, *Corros. Sci.*, **40**, 1697 (1998).
7. E. Ghali, *Mater. Sci. Forum*, **350-351**, 261 (2000).
8. J. H. Nordlien, S. Ono, and N. Masuko, *J. Electrochem. Soc.*, **142**, 3320 (1995).
9. G. L. Makar and J. Kruger, *Int. Mater. Rev.*, **38**, 138 (1993).
10. J. H. Nordlien, K. Nisancioglu, S. Ono, and N. Masuko, *J. Electrochem. Soc.*, **144**, 461 (1997).
11. O. Lunder, T. Kr. Aune, and K. Nisancioglu, *Corrosion (Houston)*, **43**, 291 (1987).
12. H. A. Evangelides, U.S. Pat. 2,723,952 (1955).
13. The Dow Chemical Company, GB Pat. 762, 195 (1956).
14. O. Khaselev, D. Weiss, and J. Yahalom, *J. Electrochem. Soc.*, **146**, 1757 (1999).
15. O. Khaselev and J. Yahalom, *J. Electrochem. Soc.*, **145**, 190 (1998).
16. A. J. Zozulin and D. E. Bartak, *Met. Finish.*, **1994**, 39 (March).
17. F. A. Bonilla, A. Berkani, Y. Liu, P. Skeldon, G. E. Thompson, H. Habazaki, K. Shimizu, C. John, and K. Stevens, *J. Electrochem. Soc.*, **149**, B4 (2002).
18. E. L. Schmeling, B. Roschenbleck, and M. H. Weidemann, U.S. Pat. 4,978,432.
19. M. Weiner, *Met. Finish.*, **93**, 65 (1995).
20. F. Mansfeld, S. Kim, and S. Lin, *J. Coat. Technol.*, **61**, 33 (1989).
21. R. G. Rateick, Jr., S. J. Xia, and V. I. Birss, in *Magnesium Technology*, H. I. Kaplan, Editor, pp. 289-294, TMS, Warrendale, PA (2002).
22. J. H. Hawkins, *The 50th Annual World Magnesium Conference*, IMA, Washington, DC, May 1993.
23. V. I. Birss, S. J. Xia, R. Yue, and R. G. Rateick, Jr., *J. Electrochem. Soc.*, **151**, B1 (2004).
24. M. Pourbaix, *Atlas of Electrochemical Equilibria in Aqueous Solutions*, NACE, Houston, TX (1974).
25. B. A. Boukamp, *Equivalent Circuit*, University of Twente, The Netherlands (1988/89).
26. M. Leibig and T. Halsey, *Electrochim. Acta*, **38**, 1985 (1993).
27. R. D. Armstrong and R. A. Burnham, *J. Electroanal. Chem. Interfacial Electrochem.*, **257**, 72 (1978).
28. R. Yue, Master Thesis, University of Calgary, Calgary, Canada (1997).
29. T. Gourley and W. H. Runciman, *J. Phys. C*, **6**, 583 (1973).
30. H. Yasuda, Q. S. Yu, and M. Chen, *Prog. Org. Coat.*, **41**, 273 (2001).
31. B. Van der Linden, H. Terryn, and J. Vereecken, *J. Appl. Electrochem.*, **20**, 798 (1990).
32. G. R. Schuller, S. R. Taylor, and E. E. Hajcsar, *J. Electrochem. Soc.*, **139**, 2799 (1992).